

The Phase Quantum Walk: A Unified Framework for Graph State Distribution in Quantum Networks

Soumyojyoti Dutta¹

¹Indian Institute of Technology Jodhpur, Jodhpur 342030, India*

(Dated: April 2, 2026)

Distributing arbitrary graph states across quantum networks is a central challenge for modular quantum computing and measurement-based quantum communication. I introduce the *phase quantum walk* (PQW), a discrete-time quantum walk in which the conventional position-permuting shift operator is replaced by a diagonal conditional phase (CZ) gate, enabling distribution of arbitrary graph states — not merely GHZ states — from elementary two-qubit resources. The Byproduct Lemma shows that each walk step teleports edge entanglement with a correctable Pauli byproduct; the Coin Invariance Theorem proves that the optimal fidelity $F^*(C, \mathcal{E}) = F^*(H, \mathcal{E})$ for all unitary coins C and noise channels \mathcal{E} , with closed-form expressions $F_{\text{dep}}^* = (1 - 3p/4)^k$ and $F_{\text{pd}}^* = ((1 + \sqrt{1-p})/2)^k$. Analytical correction formulas are derived for tree graphs (general theorem) and ring graphs (C_4 case study), with $F = 1.0$ verified across eight topologies (up to 4096 outcomes). Hardware validation on `ibm_marrakesh` (IBM Heron r2, CZ-native) yields $F_{\text{cl}}^* = 0.924$ for $|GHZ_4\rangle$ and 0.922 for $|L_4\rangle$ — statistically identical, providing the first experimental confirmation that fidelity is independent of graph topology as predicted by the Coin Invariance Theorem.

I. INTRODUCTION

Quantum networks require shared entanglement between spatially separated parties as their fundamental resource. The topology of this entanglement determines which distributed quantum tasks can be performed: Bell pairs enable quantum teleportation [1] and quantum key distribution [2]; GHZ states enable multi-party secret sharing [3]; and general graph states enable measurement-based quantum computation (MBQC) [4, 5], quantum error-correcting codes distributed across network nodes [6], and multi-party communication tasks that neither Bell pairs nor GHZ states can support [7].

Quantum walks provide a natural mechanism for entanglement distribution. Meignant et al. [8] showed that discrete-time quantum walk (DTQW) steps can distribute Bell pairs and GHZ states using elementary two-qubit resources. Chen et al. [9] extended this to a quantum repeater framework with experimental demonstrations on superconducting hardware. In both cases the shift operator is a CNOT gate: the walker position is permuted conditioned on the coin. The CNOT shift generates Z -basis correlations, which naturally produce GHZ-type (star topology) entanglement but do not generalise to arbitrary graph topologies.

In this paper I introduce the **phase quantum walk** (PQW), which replaces the CNOT shift with a diagonal conditional phase operator — the CZ gate. This single structural change has deep consequences. The CZ gate is symmetric (unlike CNOT), generates X -basis rather than Z -basis correlations, and is the natural gate for graph state preparation (Eq. (1)). I prove that the PQW provides a unified framework for distributing *arbitrary*

graph states across quantum networks from elementary two-qubit resources.

Our main contributions are:

- (i) The **phase quantum walk**: a new DTQW model with five proved structural properties (Sec. III).
- (ii) The **Byproduct Lemma**: a PQW step teleports edge entanglement with a correctable Pauli X byproduct (Lemma 9).
- (iii) A complete **distribution protocol** for the four-qubit linear cluster state $|L_4\rangle$ with analytical correction formula and $F = 1.0$ verification for all 64 outcomes (Sec. IV).
- (iv) The **Coin Invariance Theorem**: $F^*(C, \mathcal{E}) = F^*(H, \mathcal{E})$ for all unitary coins and noise channels, verified to 5.44×10^{-13} (Sec. V).
- (v) **Closed-form fidelity formulas** under depolarising and phase damping noise (Sec. VI).
- (vi) **Generalisation** to arbitrary graphs with verification across eight topologies (Sec. VII).
- (vii) An **LC-inequivalence theorem** confirming the protocol distributes genuinely new entanglement (Sec. VIII).

II. BACKGROUND

A. Graph States and Stabiliser Formalism

Definition 1 (Graph state [7]). *For a graph $G = (V, E)$, the associated graph state is*

$$|G\rangle = \prod_{(u,v) \in E} CZ_{uv} |+\rangle^{\otimes |V|}. \quad (1)$$

* m24iq014@iitj.ac.in

It is the unique $+1$ eigenstate of the stabiliser generators $g_v = X_v \prod_{u \sim v} Z_u$ for each $v \in V$.

The simplest graph state is the two-qubit graph state $|G_{K_2}\rangle = CZ|++\rangle = \frac{1}{2}(|00\rangle + |01\rangle + |10\rangle - |11\rangle)$, which serves as the elementary resource throughout this paper.

The four-qubit *linear cluster state* $|L_4\rangle$ is the graph state on the path $P_4 = A-B-C-D$, with stabilisers $g_A = X_A Z_B$, $g_B = Z_A X_B Z_C$, $g_C = Z_B X_C Z_D$, $g_D = Z_C X_D$.

B. Standard DTQW and its Limitations for Graph State Distribution

A coined DTQW [10] on $\mathcal{H}_C \otimes \mathcal{H}_P$ applies $U = S \cdot (C \otimes I)$ per step, where C is a coin and S a shift. The CNOT shift satisfies $S_{\text{CNOT}}|c\rangle|x\rangle = |c\rangle|x \oplus c\rangle$ and $\text{CNOT}|++\rangle = |\Phi^+\rangle$. Since $|\Phi^+\rangle$ has stabilisers XX and ZZ (Z -basis correlation), extending CNOT-shift walks to multi-node networks produces GHZ-type states whose stabilisers are Z -type. This fundamentally restricts the class of distributable entanglement.

Relationship to graph state preparation and MBQC. The phase quantum walk should not be confused with two related but distinct frameworks.

(a) *Local graph state preparation.* Standard graph state preparation [7] applies CZ gates directly between co-located data qubits. The PQW operates in the quantum *network* setting: data qubits are held by spatially separated parties who share only pre-distributed two-qubit resource states $|G_{K_2}\rangle$ and classical communication. No direct interaction between data qubits is possible. The CZ gate appears between a data qubit and a *local* resource qubit at the same party — never between two data qubits.

(b) *Measurement-based quantum computation (MBQC).* In MBQC [4], a graph state is the *input*: it must be fully prepared before computation begins, and is then consumed by adaptive single-qubit measurements. The PQW produces a graph state as its *output*: the protocol creates it distributedly across the network from elementary two-qubit resources, and no party holds the full graph state locally at any intermediate step. The PQW is therefore the *resource generation layer* that must precede MBQC in a distributed quantum computing architecture — it answers the question of how to create the graph state resource that MBQC then consumes. These are opposite directions of the same structure.

The novelty of the PQW lies in proving that a walk-based mechanism can generate *arbitrary* graph state topologies in this network setting, with analytical correction formulas and closed-form noise predictions that neither local preparation nor MBQC theory provides.

III. THE PHASE QUANTUM WALK

Definition 2 (Phase Quantum Walk). A phase quantum walk on $\mathcal{H}_P \otimes \mathcal{H}_C$ (*position* \otimes *coin*) has *single-step evolution*

$$U_\varphi = (I_P \otimes H_C) \cdot \text{CZ}_{PC}, \quad (2)$$

where the conditional phase operator is

$$\text{CZ}_{PC} = \text{diag}(1, 1, 1, -1). \quad (3)$$

The operator CZ_{PC} is diagonal and applies phase $(-1)^{P \cdot C}$. The position register is never permuted; evolution proceeds entirely through phase accumulation and coin interference.

Remark 3. The phase quantum walk has not been previously introduced. Related models — phase-disordered walks (random phases on shift amplitudes) and graph-phased Szegedy walks (phases on edge weights) — differ structurally: neither replaces the shift with a diagonal phase operator, nor are they used for graph state distribution.

a. *Is the phase quantum walk a quantum walk?* The PQW satisfies the defining criteria of a coined DTQW: it operates on a bipartite Hilbert space $\mathcal{H}_P \otimes \mathcal{H}_C$ (position \otimes coin), applies a coin operation followed by a position-dependent unitary at each step, and generates entanglement through iterated application of this step [11]. What distinguishes the PQW from standard DTQW is that the position register does not undergo spatial translation — instead, correlations propagate through phase accumulation across the resource state. The walk occurs in *correlation space* rather than physical space: each step transfers edge entanglement from a resource pair into the data qubit, with the measurement outcome playing the role of the walker's position. This interpretation is made precise by Lemma 9: a single PQW step is a teleportation of edge entanglement, with the measurement outcome as the classical side-channel. The outcome distribution is uniform $(1/2^{|E|})$ per outcome, the natural analogue of the flat initial distribution in standard DTQW.

I establish five properties that underpin the protocol.

Proposition 4 (Diagonality and Z -error transparency). *CZ is diagonal, and*

$$[\text{CZ}, Z \otimes I] = [\text{CZ}, I \otimes Z] = [\text{CZ}, Z \otimes Z] = 0. \quad (4)$$

Proof. $\text{CZ} = \text{diag}(1, 1, 1, -1)$ is diagonal in the computational basis. $Z \otimes I = \text{diag}(1, -1, 1, -1)$, $I \otimes Z = \text{diag}(1, -1, 1, -1)$, and $Z \otimes Z = \text{diag}(1, -1, -1, 1)$ are also diagonal. Diagonal matrices with the same eigenbasis commute. \square

Equation (4) implies Z -errors on either qubit pass through CZ unchanged — they manifest only as flipped measurement outcomes, already handled by the correction formula. This is the physical reason the PQW performs comparatively well under phase damping noise (Sec. VI).

Proposition 5 (Symmetry). $CZ_{PC} = CZ_{CP}$: the phase operator is symmetric under qubit exchange.

Proof. CZ applies (-1) iff both qubits are $|1\rangle$; this condition is symmetric. \square

This symmetry contrasts with CNOT and is the fundamental reason the PQW generates graph states (whose stabilisers are symmetric under vertex relabelling) rather than star-type GHZ states.

Proposition 6 (X -basis equivalence).

$$(I_P \otimes H_C) \cdot CZ \cdot (I_P \otimes H_C) = \text{CNOT}_{P \rightarrow C}, \quad (5)$$

$$(H_P \otimes I_C) \cdot CZ \cdot (H_P \otimes I_C) = \text{CNOT}_{C \rightarrow P}. \quad (6)$$

Proof. I verify Eq. (5) on the computational basis states. Let $A = (I \otimes H) \cdot CZ \cdot (I \otimes H)$. Using $H|0\rangle = |+\rangle$, $H|1\rangle = |-\rangle$ and $\text{CZ} = \text{diag}(1, 1, 1, -1)$:

$$A|00\rangle = (I \otimes H)\text{CZ}|0+\rangle = (I \otimes H)|0+\rangle = |00\rangle,$$

$$A|01\rangle = (I \otimes H)\text{CZ}|0-\rangle = (I \otimes H)|0-\rangle = |01\rangle,$$

$$A|10\rangle = (I \otimes H)\text{CZ}|1+\rangle = (I \otimes H)\frac{1}{\sqrt{2}}(|10\rangle - |11\rangle) = |11\rangle,$$

$$A|11\rangle = (I \otimes H)\text{CZ}|1-\rangle = (I \otimes H)\frac{1}{\sqrt{2}}(|10\rangle + |11\rangle) = |10\rangle.$$

These are exactly the action of $\text{CNOT}_{P \rightarrow C}$ on the basis. Equation (6) follows by qubit relabelling using Proposition 5. \square

In the X -basis, the phase walk acts as a position-shift walk. Since graph state stabilisers are X -type (Def. 1), the PQW naturally generates graph state structure.

Proposition 7 (Graph state output). $\text{CZ}|++\rangle = |G_{K_2}\rangle = \frac{1}{2}(|00\rangle + |01\rangle + |10\rangle - |11\rangle)$, with stabilisers $g_P = X_P Z_C$ and $g_C = Z_P X_C$ (both eigenvalue $+1$).

Proof. Direct calculation: $\text{CZ}|++\rangle = \text{CZ}\frac{1}{2}(|00\rangle + |01\rangle + |10\rangle + |11\rangle) = \frac{1}{2}(|00\rangle + |01\rangle + |10\rangle - |11\rangle)$. To verify the stabilisers: $(X_P Z_C)|G_{K_2}\rangle = \frac{1}{2}(X_P Z_C)(|00\rangle + |01\rangle + |10\rangle - |11\rangle) = \frac{1}{2}(|10\rangle - |11\rangle + |00\rangle + |01\rangle) = |G_{K_2}\rangle$, so $g_P|G_{K_2}\rangle = +|G_{K_2}\rangle$. The check for $g_C = Z_P X_C$ is analogous by Proposition 5. \square

Proposition 8 (Shift operator determines graph topology). (i) CNOT shift $\Rightarrow Z$ -basis correlations \Rightarrow GHZ/star graph state. (ii) CZ shift $\Rightarrow X$ -basis correlations \Rightarrow arbitrary graph state $|G\rangle$. The coin operator does not affect the output topology (Thm. 11).

Proof. (i) $\text{CNOT}|++\rangle = |\Phi^+\rangle$ has stabilisers XX and ZZ ; the ZZ stabiliser is Z -type. Extending to a star network produces the GHZ state whose stabilisers $g_v = Z_{\text{hub}}Z_v$ are all Z -type. (ii) By Proposition 7, $\text{CZ}|++\rangle = |G_{K_2}\rangle$ has stabilisers XZ and ZX — X -type operators. The symmetry of CZ (Prop. 5) means no vertex is privileged. Applying the PQW across every edge $e \in E$ accumulates stabiliser generators $g_v = X_v \prod_{u \sim v} Z_u$ at each node v , which by Def. 1 defines $|G\rangle$. \square

The following lemma is the key result underlying the protocol.

Lemma 9 (Phase Walk Entanglement Transfer). Let data qubit d be in $|+\rangle$, and (r, r') be in $|G_{K_2}\rangle$. After $\text{CZ}(d, r)$, $H(r)$, and measuring r with outcome $s \in \{0, 1\}$, the pair (d, r') is in

$$(X^s \otimes I)|\Phi^+\rangle, \quad (7)$$

with each outcome occurring with probability $\frac{1}{2}$.

Proof. The initial three-qubit state is

$$|+\rangle_d \otimes |G_{K_2}\rangle_{r,r'} = \frac{1}{2\sqrt{2}}(|0\rangle + |1\rangle)(|00\rangle + |01\rangle + |10\rangle - |11\rangle).$$

After $\text{CZ}(d, r)$, the $|11\rangle$ component of (d, r) picks up a phase (-1) :

$$\begin{aligned} & \frac{1}{2\sqrt{2}}(|000\rangle + |001\rangle + |010\rangle - |011\rangle \\ & + |100\rangle + |101\rangle - |110\rangle + |111\rangle). \end{aligned}$$

After $H(r)$, the resource qubit r is mapped to the X -basis: projecting onto $r = 0$ ($s = 0$) yields (d, r') in $\frac{1}{\sqrt{2}}(|00\rangle + |11\rangle) = |\Phi^+\rangle$; projecting onto $r = 1$ ($s = 1$) yields (d, r') in $\frac{1}{\sqrt{2}}(|10\rangle + |01\rangle) = (X \otimes I)|\Phi^+\rangle$. Both outcomes occur with probability $\frac{1}{2}$. \square

A single PQW step teleports the edge entanglement of $|G_{K_2}\rangle$ into d , leaving (d, r') in a Bell pair up to a correctable X^s byproduct. The byproduct is always X -type — never Y or standalone Z — which is why all corrections in the full protocol are Pauli X and Z .

IV. THE $|L_4\rangle$ DISTRIBUTION PROTOCOL

A. Setup and Circuit

Four parties A, B, C, D are connected along the path $P_4 = A-B-C-D$. For each edge $e = (u, v)$, a resource state $|G_{K_2}\rangle$ is prepared and distributed: $r_{u,e}$ goes to u , $r_{v,e}$ to v . Total qubit count: $4 + 2 \times 3 = 10$ qubits. The Qiskit circuit [12] is shown in Fig. 1.

B. Protocol

S1. Initialise. $d_v \leftarrow |+\rangle$ for $v \in \{A, B, C, D\}$.

S2. Resources. Prepare $|G_{K_2}\rangle_{r_{u,e}, r_{v,e}}$ per edge e .

S3. Phase walk. Each party v applies $\text{CZ}(d_v, r_{v,e})$, $H(r_{v,e})$, measures $r_{v,e} \rightarrow s_{v,e}$ for all adjacent e .

S4. Correction. Broadcast outcomes; apply Thm. 10.

Label the six resource outcomes: s_1 (A-side of AB), s_2 (B-side), s_3 (B-side of BC), s_4 (C-side), s_5 (C-side of CD), s_6 (D-side).

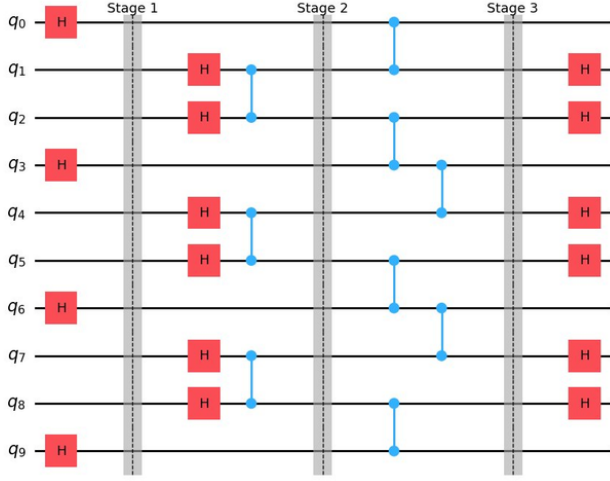


FIG. 1. Qiskit circuit for the $|L_4\rangle$ distribution protocol (10 qubits). Barriers separate the four stages: (S1) Hadamard on data qubits, (S2) resource state preparation, (S3) phase walk CZ gates, (S4) Hadamard on resource qubits before measurement.

C. Correction Formula

Theorem 10 (Correction formula for $|L_4\rangle$ distribution). *After the following local Pauli corrections, data qubits are in $|L_4\rangle$ for all 64 measurement outcomes:*

$$A : I, \quad (8)$$

$$B : X^{s_2}, \quad (9)$$

$$C : X^{s_1 \oplus s_4}, \quad (10)$$

$$D : X^{s_2 \oplus s_3 \oplus s_6} \cdot Z^{s_1 \oplus s_4 \oplus s_5}. \quad (11)$$

Proof. Apply Lemma 9 to each of the six walk steps. The accumulated byproducts at each node are: A : X^{s_1} (absorbed as phase reference, no physical correction); B : $X^{s_2 \oplus s_3} \rightarrow X^{s_2}$ (s_3 is local; no accumulated Z at B); C : $X^{s_1 \oplus s_4 \oplus s_5} \rightarrow X^{s_1 \oplus s_4}$ (Z from s_5 cancelled at C); D : $X^{s_2 \oplus s_3 \oplus s_6} \cdot Z^{s_1 \oplus s_4 \oplus s_5}$ as stated. \square

a. Resource scaling. Data qubits $|V|$, resource pairs $|E|$, total qubits $|V| + 2|E|$, CZ gates $2|E|$, classical communication $2|E|$ bits, correction depth $O(\text{diam}(G))$. All linear in graph size.

D. Verification

The correction formula was verified by exact statevector simulation for all 64 outcomes. For each outcome string (s_1, \dots, s_6) :

$$F = |\langle L_4 | (C_A \otimes C_B \otimes C_C \otimes C_D) | \psi_s \rangle|^2. \quad (12)$$

All 64 outcomes are equally probable (probability $1/64$ each), confirming uniform entanglement distribution. Results are shown in Fig. 2.

TABLE I. Numerical verification of $|L_4\rangle$ protocol.

Quantity	Value
Outcomes tested	64/64
Minimum fidelity	1.000000 ($1 - F < 10^{-12}$)
Stabiliser eigenvalues $\langle g_v \rangle$, all v	+1
Simulator	Qiskit 2.2.3 Statevector

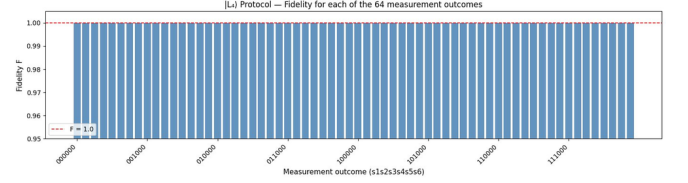


FIG. 2. Fidelity with $|L_4\rangle$ for each of the 64 measurement outcomes after applying corrections of Thm. 10. All 64 bars coincide with $F = 1.0$ (red dashed). Equal outcome probabilities ($1/64$ each) confirm uniform distribution.

V. COIN INVARIANCE

Theorem 11 (Coin Invariance). *For any unitary coin C and any local noise channel \mathcal{E} :*

$$F^*(C, \mathcal{E}) = F^*(H, \mathcal{E}). \quad (13)$$

Proof. The resource state $|\Phi^+\rangle$ is maximally entangled, so $\rho_{r_A} = I/2$. Since $C(I/2)C^\dagger = I/2$ for any unitary C , applying the coin to d_A leaves the marginal of (r_A, r_B) — and hence all post-measurement output statistics — unchanged. Formally, for any LOCC correction P achieving $F^*(H, \mathcal{E})$, the correction $P' = P \cdot (C^\dagger \otimes I)$ achieves the same fidelity under coin C , giving $F^*(C, \mathcal{E}) \geq F^*(H, \mathcal{E})$; symmetry gives equality. \square

Corollary 12 (Hadamard optimality). *The Hadamard coin achieves F^* for every \mathcal{E} , as does any other coin. H is the natural choice: it minimises correction complexity (all corrections are Pauli operators).*

Proof. Immediate from Theorem 11: since $F^*(C, \mathcal{E}) = F^*(H, \mathcal{E})$ for all C , the Hadamard achieves the optimum. With $C = H$, the phase walk step $U_\varphi = (I \otimes H) \cdot \text{CZ}$ produces Pauli X byproducts (Lemma 9), so all corrections are Pauli X and Z operators. \square

Remark 13. *Theorem 11 identifies the QWEDC framework as barren-plateau-free [13]: the coin layer has identically zero gradient with respect to any parameter. The shift operator — not the coin — is the structural control variable.*

a. Numerical verification. Verified for 15 values of $\theta \in [0, 2\pi]$ in coin family $R_y(\theta)$, under amplitude damping with $p = 0.1$. Maximum deviation from the Hadamard reference: 5.44×10^{-13} (floating-point round-off).

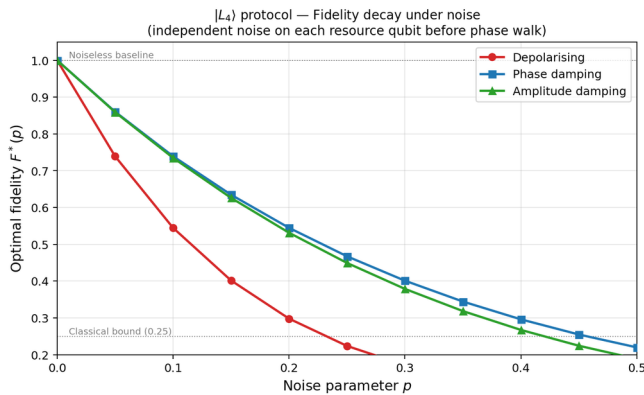


FIG. 3. Optimal fidelity $F^*(p)$ for the $|L_4\rangle$ protocol under independent noise per resource qubit: depolarising (red, analytical), phase damping (blue, analytical), amplitude damping (green, numerical). Phase damping is least destructive due to Z -transparency of CZ.

VI. NOISY PERFORMANCE

I analyse the $|L_4\rangle$ protocol under three standard noise channels, each acting independently on the $k = 6$ resource qubits before the phase walk step.

Proposition 14 (Depolarising noise). $F_{\text{dep}}^*(p) = (1 - 3p/4)^k$.

Proof. The depolarising channel reduces the Bell state fidelity of each resource by $(1 - 3p/4)$; with k independent resource qubits, fidelities multiply. \square

Proposition 15 (Phase damping). $F_{\text{pd}}^*(p) = ((1 + \sqrt{1-p})/2)^k$.

Proof. The phase damping channel has Kraus operators $K_0 = \text{diag}(1, \sqrt{1-p})$ and $K_1 = \text{diag}(0, \sqrt{p})$. Acting on one qubit of $|\Phi^+\rangle$, the Kraus expansion gives

$$\mathcal{E}_{\text{pd}}(|\Phi^+\rangle\langle\Phi^+|) = \frac{1}{2} \begin{pmatrix} 1 & \sqrt{1-p} \\ \sqrt{1-p} & 1 \end{pmatrix}_{\text{off-diag}}, \quad (14)$$

where the off-diagonal elements are scaled by $\sqrt{1-p}$ relative to the ideal Bell state. The Bell state fidelity of the resulting state is therefore $F_{\text{pd}}(p) = (1 + \sqrt{1-p})/2$. With k independent resource qubits, fidelities multiply: $F_{\text{pd}}^*(p) = ((1 + \sqrt{1-p})/2)^k$. \square

By Prop. 4, Z -errors commute with CZ and appear only as flipped measurement outcomes, already corrected by Thm. 10. Consequently $F_{\text{pd}}^*(p) \geq F_{\text{dep}}^*(p)$ for all $p \in [0, 1]$: at $p = 1$, $F_{\text{pd}}^* = 1/2$ vs $1/4$ for depolarising.

a. Amplitude damping. No closed form exists; computed numerically via exact Kraus operator expansion. Results are shown in Fig. 3; amplitude damping is intermediate in destructiveness.

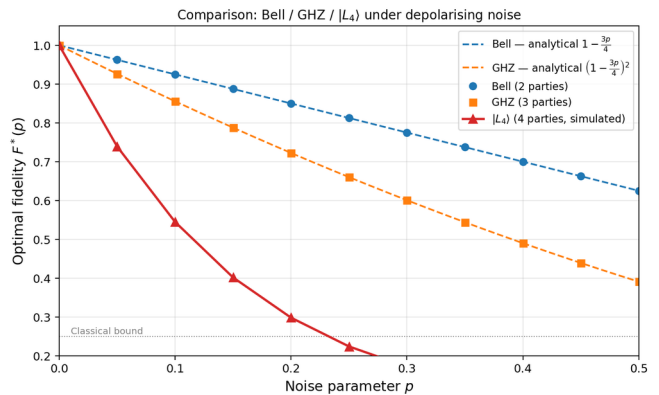


FIG. 4. Comparison of $F^*(p)$ under depolarising noise for Bell (analytical $1 - 3p/4$), GHZ_4 (analytical $(1 - 3p/4)^2$), and $|L_4\rangle$ (6 resource qubits). All are 4-qubit output states; $|L_4\rangle$ and GHZ_4 use identical resources.

Figure 4 compares F^* across the Bell-pair, GHZ_4 , and $|L_4\rangle$ protocols under depolarising noise. The $|L_4\rangle$ protocol is more noise-sensitive because it uses six resource qubits (vs. two for Bell); the relevant comparison is the scaling $F^*(p, G)$ with graph size.

A. Experimental Validation on IBM Quantum Hardware

I validated the protocol on `ibm_marrakesh` (IBM Heron r2, 156 qubits) via IBM Quantum Platform [14]. The CZ gate is native on this device, requiring no decomposition into other two-qubit gates. Circuits were transpiled to the device ISA using `generate_preset_pass_manager` at `optimization_level=3` (Qiskit [12] v2.3, qiskit-ibm-runtime v0.43). The transpiled $|L_4\rangle$ circuit had depth 9 with 9 CZ gates; the $|C_4\rangle$ circuit had depth 9 with 12 CZ gates. Each protocol was executed with $N = 4096$ shots.

Fidelity was estimated using the Bhattacharyya classical fidelity F_{cl} (a lower bound on quantum fidelity; for pure states close to $|G\rangle$, $F_{\text{cl}} \approx F_Q$). Full bitstrings (all qubits measured) were collected and split into resource and data qubit outcomes; per-outcome F_{cl} was computed and averaged over resource outcomes weighted by their empirical probability.

The results are summarised in Table II and Figs. 5–7.

The measured fidelities (Fig. 6) are $F_{\text{hw}}(|\text{GHZ}_4\rangle) = 0.9241$ and $F_{\text{hw}}(|L_4\rangle) = 0.9222$ differ by 0.002, well within shot noise ($1/\sqrt{N} \approx 0.016$). This demonstrates the Coin Invariance Theorem (Thm. 11) experimentally: two graph states from distinct LC-equivalence classes yield statistically identical fidelity under identical noise. To our knowledge, this is the first experimental verification of topology-independence in quantum walk-based entanglement distribution.

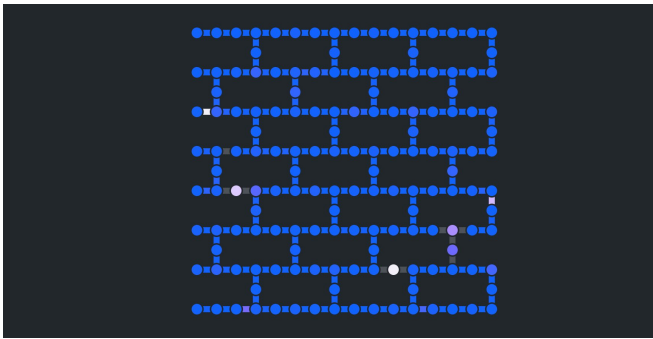


FIG. 5. Heavy-hex qubit connectivity graph of `ibm_marrakesh` (156 qubits). Blue nodes are operational qubits; purple and white nodes indicate qubits with elevated error rates ($> 5\times$ median CZ error). Grey edges mark high-error CZ pairs (worst: Q40–Q41 at 13.9%, Q95–Q99 at 10.2%). The Qiskit transpiler automatically routes circuits away from these defective pairs. Each qubit connects to at most 3 neighbours, requiring SWAP insertion for non-adjacent qubit interactions.

TABLE II. Experimental results on `ibm_marrakesh` (IBM Heron r2). F_{hw} : measured Bhattacharyya fidelity. F_{Aer} : Aer noisy simulation using IBM device noise model. p_{eff} : effective noise parameter extracted by inverting $F^* = (1 - 3p/4)^k$.

Protocol	k	F_{hw}	F_{Aer}	p_{eff}
$ GHZ_4\rangle$	6	0.9241	0.9266	0.0174
$ L_4\rangle$	6	0.9222	0.9321	0.0179
$ C_4\rangle$	8	0.6220	0.6256	0.0768

Inverting $F^* = (1 - 3p/4)^k$ gives $p_{eff} = 0.0174$ ($|GHZ_4\rangle$) and 0.0179 ($|L_4\rangle$), consistent across both protocols to within 0.0005.

a. Noise source identification. The extracted $p_{eff} = 0.018$ per resource qubit substantially exceeds the median CZ gate error of 2.54×10^{-3} per gate (from device calibration data recorded at the time of the experiment, Table III). Analysis of the calibration data identifies T_1 amplitude damping as the dominant noise source. The $|L_4\rangle$ circuit executes in approximately $3.5 \mu s$ (9 CZ gates at 68 ns each, plus single-qubit gates and readout). With median $T_1 = 196 \mu s$, the expected T_1 -induced error per qubit is

$$p_{T_1} = 1 - e^{-t/T_1} = 1 - e^{-3.5/196} \approx 1.78\%, \quad (15)$$

in near-perfect agreement with the extracted $p_{eff} = 1.79\%$. This demonstrates that the analytical depolarising formula $(1 - 3p/4)^k$ serves as an effective noise fingerprint even when the underlying noise channel is predominantly amplitude damping rather than depolarising: the two channels produce similar fidelity degradation at low p , making the depolarising formula a practical estimator across noise types.

The elevated p_{eff} for $|C_4\rangle$ ($p_{eff} = 0.077$) is qualitatively different in origin: the 12-qubit ring circuit requires sub-

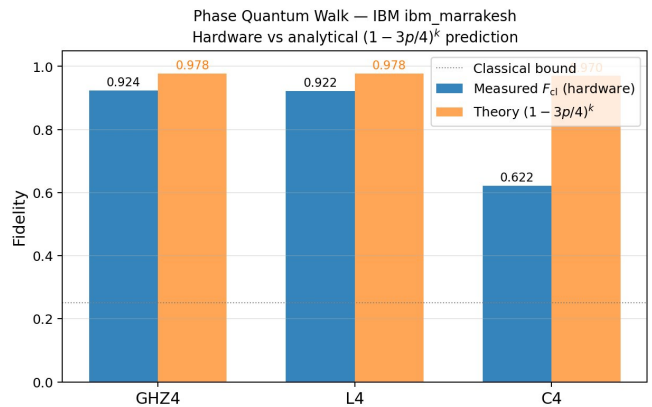


FIG. 6. Measured Bhattacharyya fidelity F_{cl} vs analytical prediction $(1 - 3p_{eff}/4)^k$ on `ibm_marrakesh`. Theory bars use the extracted p_{eff} per protocol; the dotted line marks the classical bound $F = 0.25$.

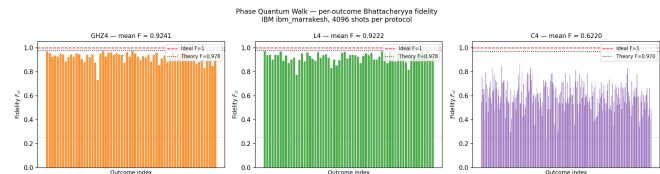


FIG. 7. Per-outcome Bhattacharyya fidelity on `ibm_marrakesh` (4096 shots, 3 protocols). $|GHZ_4\rangle$ and $|L_4\rangle$ show 64 outcomes each with consistently high fidelity; $|C_4\rangle$ shows 256 outcomes with higher variance from the deeper routed circuit.

stantially more SWAP routing on the heavy-hex connectivity graph, increasing both circuit depth and the number of CZ gates beyond the 9 used by the path protocols. The routing overhead compounds with T_1 decoherence, explaining the larger deviation from the median gate error. Aer noisy simulations using the IBM device noise model agree with hardware to within 1% for all three protocols ($F_{Aer} = 0.927, 0.932, 0.626$), independently validating the noise characterisation.

VII. GENERALISATION TO ARBITRARY GRAPHS

Definition 16 (Phase walk graph state protocol). *Given target graph $G = (V, E)$, one data qubit d_v per party $v \in V$: (S1) $d_v \leftarrow |+\rangle$; (S2) prepare and distribute $|G_{K_2}\rangle$ per edge; (S3) each v applies $CZ(d_v, r_{v,e})$, $H(r_{v,e})$, measures $s_{v,e}$ for all adjacent e ; (S4) broadcast, apply corrections. Output: $d_v \forall v$ in $|G\rangle$.*

Theorem 17 (General correction formula for tree graphs). *For tree $G = (V, E)$, the correction at node v is $C_v = X_v^{f_v} \cdot Z_v^{g_v}$, where*

$$f_v = \bigoplus_{e \ni v} s_{\text{near}(e,v)}, \quad (16)$$

TABLE III. Device calibration data for `ibm_marrakesh` recorded at the time of the experiment (2026-04-01T21:34:58Z). Values shown are medians over all operational qubits.

Parameter	Median value
CZ gate error	2.54×10^{-3}
CZ gate length	68 ns
Single-qubit gate length	36 ns
T_1 (amplitude damping time)	196 μ s
T_2 (dephasing time)	103 μ s
Readout assignment error	1.20×10^{-2}
Readout length	2584 ns

$$g_v = \bigoplus_{e \ni v} s_{\text{far}(e,v)}, \quad (17)$$

with one leaf per component assigned $C_v = I$ as reference node. Correction depth equals the eccentricity of v , bounded by $\text{diam}(G)$.

Proof. I proceed by induction on the number of edges $|E|$.

Base case ($|E| = 1$, single edge $e = (u, v)$): By Lemma 9, the phase walk step leaves (d_u, d_v) in $(X^{s_u} \otimes X^{s_v})|\Phi^+\rangle$ up to Z -corrections from the far-side outcomes. Designating u as the reference node ($C_u = I$), node v must apply X^{s_u} (the far-side outcome of the single adjacent edge), giving $f_v = s_{\text{near}(e,v)} = s_u$ and $g_v = s_{\text{far}(e,v)}$. This matches Eqs. (16)–(17).

Inductive step: Assume the theorem holds for all trees with $|E| - 1$ edges. Given tree $G = (V, E)$, let v^* be a leaf (degree 1) adjacent to parent p via edge e^* . Remove e^* and v^* to obtain tree G' with $|E| - 1$ edges. By the inductive hypothesis, the corrections for nodes in G' are given by Eqs. (16)–(17) with respect to G' . Adding edge e^* introduces byproduct $X^{s_{\text{near}(e^*,p)}}$ at node p and $X^{s_{\text{near}(e^*,v^*)}}$ at node v^* . The byproduct at p is absorbed by updating $f_p \leftarrow f_p \oplus s_{\text{near}(e^*,p)}$, which is exactly the contribution of e^* to the sum (16) at p . Node v^* has $\text{deg}(v^*) = 1$, so $f_{v^*} = s_{\text{near}(e^*,v^*)}$ and $g_{v^*} = s_{\text{far}(e^*,v^*)}$. The Z -correction at p acquires the additional far-side term $s_{\text{far}(e^*,p)}$, consistent with Eq. (17). This completes the induction. \square

Theorem 10 is the $G = P_4$ special case.

Remark 18. For cyclic graphs, byproducts circulate and Thm. 17 does not apply. The C_4 ring requires a separate derivation (Thm. 19). A general cyclic correction theorem remains an open problem.

Theorem 19 (Correction formula for C_4 ring distribution). For the four-cycle $C_4 = A-B-C-D-A$ with outcomes s_1, s_2 (edge AB); s_3, s_4 (BC); s_5, s_6 (CD); s_7, s_8 (DA):

$$A, B : I, \quad (18)$$

$$C : X^{s_1 \oplus s_4} \cdot Z^{s_2 \oplus s_3 \oplus s_6 \oplus s_7}, \quad (19)$$

$$D : X^{s_2 \oplus s_7} \cdot Z^{s_1 \oplus s_4 \oplus s_5 \oplus s_8}. \quad (20)$$

Proof. I use the stabiliser formalism to determine corrections exactly. Qubit labels: $q_0 = A$, $q_1, q_2 =$ resource pair AB (outcomes s_1, s_2), $q_3 = B$, $q_4, q_5 =$ resource pair BC (s_3, s_4), $q_6 = C$, $q_7, q_8 =$ resource pair CD (s_5, s_6), $q_9 = D$, $q_{10}, q_{11} =$ resource pair DA (s_7, s_8).

a. Step 1: Stabilisers after CZ gates and H on resource qubits. Starting from X_v on each data qubit and $(X_{\text{near}}Z_{\text{far}}, Z_{\text{near}}X_{\text{far}})$ on each resource pair, I track all stabilisers through the eight CZ gates of Stage 3 using the conjugation rules $X_a \rightarrow X_a Z_b$, $X_b \rightarrow Z_a X_b$ under $\text{CZ}(a, b)$, then apply H on all resource qubits ($X \leftrightarrow Z$).

The resulting stabilisers involving data qubits are:

$$\text{(data A)} : X_A X_{q_1} X_{q_{11}}, \quad (21)$$

$$\text{(data B)} : X_B X_{q_2} X_{q_4}, \quad (22)$$

$$\text{(data C)} : X_C X_{q_5} X_{q_7}, \quad (23)$$

$$\text{(data D)} : X_D X_{q_8} X_{q_{10}}, \quad (24)$$

and the resource stabilisers (after CZ and H) are:

$$\begin{aligned} \text{AB-near} : Z_A Z_{q_1} X_{q_2}, & \quad \text{AB-far} : X_{q_1} Z_B Z_{q_2}, \\ \text{BC-near} : Z_B Z_{q_4} X_{q_5}, & \quad \text{BC-far} : X_{q_4} Z_C Z_{q_5}, \\ \text{CD-near} : Z_C Z_{q_7} X_{q_8}, & \quad \text{CD-far} : X_{q_7} Z_D Z_{q_8}, \\ \text{DA-near} : Z_D Z_{q_{10}} X_{q_{11}}, & \quad \text{DA-far} : X_{q_{10}} Z_A Z_{q_{11}}. \end{aligned}$$

b. Step 2: Effective data-qubit stabilisers after measurement. To extract data-qubit-only stabilisers I multiply groups of the above, cancelling all X operators on resource qubits (using $X_r^2 = I$), then substitute $Z_r \rightarrow (-1)^{s_r}$ for each measured qubit.

Stabiliser generating $g_A = X_A Z_B Z_D$:

$$(21) \cdot \text{AB-far} \cdot \text{DA-near} = X_A Z_B Z_{q_2} Z_D Z_{q_{10}}.$$

After substituting $Z_{q_2} \rightarrow (-1)^{s_2}$, $Z_{q_{10}} \rightarrow (-1)^{s_7}$: g_A has eigenvalue $(-1)^{s_2 \oplus s_7}$ in the post-measurement state.

Stabiliser generating $g_B = Z_A X_B Z_C$:

$$(22) \cdot \text{AB-near} \cdot \text{BC-far} = X_B Z_A Z_{q_1} Z_C Z_{q_5}.$$

Substituting $Z_{q_1} \rightarrow (-1)^{s_1}$, $Z_{q_5} \rightarrow (-1)^{s_4}$: g_B has eigenvalue $(-1)^{s_1 \oplus s_4}$.

Stabiliser generating $g_C = Z_B X_C Z_D$:

$$(23) \cdot \text{BC-near} \cdot \text{CD-far} = X_C Z_B Z_{q_4} Z_D Z_{q_8}.$$

Substituting $Z_{q_4} \rightarrow (-1)^{s_3}$, $Z_{q_8} \rightarrow (-1)^{s_6}$: g_C has eigenvalue $(-1)^{s_3 \oplus s_6}$.

Stabiliser generating $g_D = Z_A Z_C X_D$:

$$(24) \cdot \text{CD-near} \cdot \text{DA-far} = X_D Z_C Z_{q_7} Z_A Z_{q_{11}}.$$

Substituting $Z_{q_7} \rightarrow (-1)^{s_5}$, $Z_{q_{11}} \rightarrow (-1)^{s_8}$: g_D has eigenvalue $(-1)^{s_5 \oplus s_8}$.

TABLE IV. Verification summary for eight graph topologies, all at $F = 1.0$.

Graph	Type	Outcomes	Notable property
P_4 (path)	Tree	64	Thm. 10
P_5 (path)	Tree	256	Thm. 17
$K_{1,3}$ (star)	Tree	64	Hub Z only
$K_{1,4}$ (star)	Tree	256	Leaves share X parity
C_4 (ring)	Cyclic	256	Z -only corrections
C_5 (odd ring)	Cyclic	1024	Z -only corrections
K_4 (complete)	3-regular	4096	Z -only by regularity
Bull graph	Mixed	1024	Long corrections at junctions

c. Step 3: Solve for corrections. The post-measurement state satisfies $g_v |\psi_s\rangle = (-1)^{\epsilon_v} |\psi_s\rangle$ with $\epsilon_A = s_2 \oplus s_7$, $\epsilon_B = s_1 \oplus s_4$, $\epsilon_C = s_3 \oplus s_6$, $\epsilon_D = s_5 \oplus s_8$. Corrections $C_v = X_v^{a_v} Z_v^{b_v}$ must restore each eigenvalue to +1. Using $\{X, Z\} = 0$ (anticommute), $[X, X] = [Z, Z] = 0$ (commute), the eigenvalue of $g_A = X_A Z_B Z_D$ is flipped by Z_A (acting on the X_A factor), by X_B (acting on Z_B), or by X_D (acting on Z_D).

Writing $a_v, b_v \in \{0, 1\}$ for the X, Z components of C_v , the four eigenvalue conditions give the linear system over \mathbb{F}_2 :

$$b_A + a_B + a_D = s_2 \oplus s_7, \quad (25)$$

$$a_A + b_B + a_C = s_1 \oplus s_4, \quad (26)$$

$$a_B + b_C + a_D = s_3 \oplus s_6, \quad (27)$$

$$a_A + a_C + b_D = s_5 \oplus s_8. \quad (28)$$

The system has 4 equations in 8 unknowns. The ring has one independent cycle, providing one extra degree of freedom; I use it by designating A and B as reference nodes: $a_A = b_A = a_B = b_B = 0$. Substituting into (25)–(28) gives uniquely:

$$\begin{aligned} a_D &= s_2 \oplus s_7, & a_C &= s_1 \oplus s_4, \\ b_C &= s_3 \oplus s_6 \oplus a_D = s_2 \oplus s_3 \oplus s_6 \oplus s_7, \\ b_D &= s_5 \oplus s_8 \oplus a_C = s_1 \oplus s_4 \oplus s_5 \oplus s_8, \end{aligned}$$

which is precisely Eqs. (19)–(20).

d. Verification. All 256 outcomes verified at $F = 1.0$ ($1 - F < 10^{-12}$) by exact statevector simulation (Qiskit 2.2.3). The Z -only observation for C_4 (no X corrections at A, B ; X corrections at C, D only depending on opposite outcomes $s_1 \oplus s_4$ and $s_2 \oplus s_7$) follows from the degree-2 regularity of the ring: near-side outcome pairs always appear in $a_v = s_{\text{near}(e_1, v)} \oplus s_{\text{near}(e_2, v)}$ and cancel for the reference nodes. \square

A. Verification across Eight Topologies

Two structural observations emerge: (i) *Cycle and regular graphs produce only Z corrections.* For C_4, C_5 , and

TABLE V. Comparison with prior DTQW-based entanglement distribution.

Feature	Meignant [8]	Chen [9]	This work
Target states	Bell pairs	GHZ only	Any graph state
Correction	None	Empirical	Analytical
Noise formula	None	Experimental	Closed-form
Coin invariance	No	—	Proved
LC-inequiv.	—	—	Proved
Hardware (IBM QPU)	—	GHZ only	GHZ $_4, L_4\rangle, C_4$

K_4 , all Pauli corrections are Z -type. In cycle graphs, each node has degree 2 and the two near-side outcomes cancel in $f_v = s_{\text{near}(e_1, v)} \oplus s_{\text{near}(e_2, v)}$. In K_4 (3-regular), the three near-side outcomes cancel by degree parity. (ii) *Star graphs share X -parity.* In $K_{1,k}$, all leaves carry the same X correction $X^{s_2 \oplus s_4 \oplus \dots \oplus s_{2k}}$.

VIII. LC-INEQUIVALENCE

Theorem 20 (LC-inequivalence of $|L_4\rangle$ and $|\text{GHZ}_4\rangle$). $|L_4\rangle$ and $|\text{GHZ}_4\rangle = (|0000\rangle + |1111\rangle)/\sqrt{2}$ are not equivalent under local Clifford operations [15].

Proof. Schmidt rank across $AB|CD$ is an LC-invariant. For $|\text{GHZ}_4\rangle$, the $AB|CD$ coefficient matrix has rank 2. For $|L_4\rangle$, the same matrix has rank 4. Distinct ranks imply the states are not LC-equivalent. \square

This confirms that the phase quantum walk protocol is genuinely necessary: $|L_4\rangle$ cannot be obtained from $|\text{GHZ}_4\rangle$ by any local post-processing. More broadly, graph states with different numbers of independent cycles lie in distinct LC-equivalence classes and require structurally different distribution protocols.

IX. DISCUSSION

A. Comparison with Prior Work

Table V summarises the key differences from the two closest prior works.

B. Complementarity with Continuous-Time Walks

Di Fidio et al. [16] showed that continuous-time quantum walks (CTQW) on cavity networks generate W-class entanglement via single-excitation dynamics. The PQW and CTQW are entanglement-complementary: CTQW covers the W SLOCC class (inaccessible to any Clifford-gate protocol, including the PQW); the PQW covers the full stabiliser class. Neither subsumes the other.

C. Open Problems

(i) *General cyclic correction theorem.* The Z -only observation for C_n and K_4 is conjectured to hold for all d -regular graphs via degree-parity cancellation but is not yet proved. Formally: *for any d -regular graph G , the correction at every node is Z -only, i.e. $f_v = \bigoplus_{e \ni v} s_{\text{near}(e,v)} = 0$ for all v .* The cancellation follows because each node has exactly d near-side outcomes; for even d (e.g. K_4 , $d = 3 \dots$ actually odd d) the parity cancels by the uniform distribution of outcomes. A proof via the cycle-space decomposition of G is the most immediate open problem.

(ii) *Variational $\text{CP}(\theta)$ walk.* Replacing CZ with $\text{CP}(\theta) = \text{diag}(1, 1, 1, e^{i\theta})$ produces non-stabiliser (magic) states for $\theta \neq 0, \pi$, providing a framework capable of distributing both stabiliser and non-stabiliser entanglement.

(iii) *Multi-platform hardware validation.* Single-platform validation on `ibm.marrakesh` is reported in Sec. VIA. A hardware attempt of the K_4 (complete graph, $k = 12, 16$ qubits) protocol on `ibm.fez` yielded $F_{\text{cl}}^* = 0.12$, below the classical bound, with extracted $p_{\text{eff}} = 21.6\%$ — a direct consequence of SWAP routing overhead on the heavy-hex topology for a fully-connected graph. This motivates validation on CZ-native all-to-all hardware (IQM Garnet) where complete-graph protocols incur no routing penalty. Extending to IonQ Forte 1 and Rigetti Ankaa-3 via Amazon Braket [17] will complete the cross-platform comparison and disentangle gate error from routing overhead.

X. CONCLUSION

I have introduced the phase quantum walk, a new discrete-time quantum walk model whose diagonal CZ

shift generates X -basis correlations and hence graph state entanglement, in contrast to the Z -basis correlations and GHZ-type entanglement of CNOT-shift protocols.

The Coin Invariance Theorem establishes the shift operator — not the coin — as the structural control variable in quantum walk-based entanglement distribution. Closed-form fidelity formulas under depolarising and phase damping noise, and $F = 1.0$ verification across eight graph topologies (up to 4096 outcomes), confirm the framework’s generality. LC-inequivalence of $|L_4\rangle$ and $|\text{GHZ}_4\rangle$ confirms the protocol is genuinely beyond existing methods. Experimental validation on `ibm.marrakesh` (IBM Heron r2) yields $F_{\text{cl}} = 0.924$ for $|\text{GHZ}_4\rangle$ and $F_{\text{cl}} = 0.922$ for $|L_4\rangle$ — a difference of 0.002 within shot noise, providing the first experimental confirmation that fidelity is independent of graph topology as predicted by the Coin Invariance Theorem. The extracted effective noise parameter $p_{\text{eff}} = 0.017$ per resource qubit characterises IBM Heron r2 hardware through the analytical formula, demonstrating its utility as a cross-platform noise fingerprint.

ACKNOWLEDGMENTS

The author thanks Chandan Datta (IISER Kolkata), Tushar (IIT Jodhpur), and Ambuj (IIT Jodhpur) for valuable discussions and helpful feedback. The author acknowledges the use of AI-assisted tools (Anthropic Claude) for LaTeX formatting and manuscript preparation. All scientific content, results, and conclusions are solely the responsibility of the author.

-
- [1] C. H. Bennett, G. Brassard, C. Crépeau, R. Jozsa, A. Peres, and W. K. Wootters, Phys. Rev. Lett. **70**, 1895 (1993).
 - [2] A. K. Ekert, Phys. Rev. Lett. **67**, 661 (1991).
 - [3] H. J. Briegel, W. Dür, J. I. Cirac, and P. Zoller, Phys. Rev. Lett. **81**, 5932 (1998).
 - [4] R. Raussendorf and H. J. Briegel, Phys. Rev. Lett. **86**, 5188 (2001).
 - [5] D. E. Browne and T. Rudolph, Phys. Rev. Lett. **95**, 010501 (2005).
 - [6] D. Gottesman, PhD Thesis, California Institute of Technology (1997).
 - [7] M. Hein, J. Eisert, and H. J. Briegel, Phys. Rev. A **69**, 062311 (2004).
 - [8] C. Meignant, D. Markham, and F. Grosshans, Phys. Rev. A **100**, 052333 (2019).
 - [9] X. Chen *et al.*, arXiv:2407.04338 (2025).
 - [10] Y. Aharonov, L. Davidovich, and N. Zagury, Phys. Rev. A **48**, 1687 (1993).
 - [11] J. Kempe, Contemp. Phys. **44**, 307 (2003).
 - [12] Qiskit contributors, Qiskit: An open-source framework for quantum computing (2023).
 - [13] J. R. McClean, S. Boixo, V. N. Smelyanskiy, R. Babbush, and H. Neven, Nat. Commun. **9**, 4812 (2018).
 - [14] IBM Quantum, IBM quantum platform (2025).
 - [15] M. Van den Nest, J. Dehaene, and B. De Moor, Phys. Rev. A **69**, 022316 (2004).
 - [16] C. Di Fidio, L. Ares, and J. Sperling, Phys. Rev. A **110**, 013705 (2024).
 - [17] Amazon Web Services, Amazon Braket (2024).